warwick.ac.uk/lib-publications

Spin-splitting in p-type Ge devices

S. N. Holmes,[1,a)] P. J. Newton,[1] J. Llandro,[1] R. Mansell,[1] C. H. W. Barnes,[1] C. Morrison,[2] and M. Myronov[2]

[1]*Cavendish Laboratory, Department of Physics, University of Cambridge, J. J. Thomson Avenue, Cambridge CB3 0HE, United Kingdom*
[2]*Department of Physics, University of Warwick, Coventry CV4 7AL, United Kingdom*

Compressively strained Ge quantum well devices have a spin-splitting in applied magnetic field that is entirely consistent with a Zeeman effect in the heavy hole valence band. The spin orientation is determined by the biaxial strain in the quantum well with the relaxed SiGe buffer layers and is quantized in the growth direction perpendicular to the conducting channel. The measured spin-splitting in the resistivity ρ_{xx} agrees with the predictions of the Zeeman Hamiltonian where the Shubnikov-deHaas effect exhibits a loss of *even* filling factor minima in the resistivity ρ_{xx} with hole depletion from a gate field, increasing disorder or increasing temperature. There is no measurable Rashba spin-orbit coupling irrespective of the structural inversion asymmetry of the confining potential in low p-doped or undoped Ge quantum wells from a density of $6 \times 10^{10}\,cm^{-2}$ in depletion mode to $1.7 \times 10^{11}\,cm^{-2}$ in enhancement. *Published by AIP Publishing.*
[http://dx.doi.org/10.1063/1.4961416]

I. INTRODUCTION

The present trend in miniaturization of complementary metal-oxide-semiconductor (CMOS) silicon devices[1] to shorter gate length and thinner oxide dielectric, following the predictions of Moore's law, has come at a cost of *reduced* performance with *increasing* power consumption.[2] Replacing Si with higher mobility Ge can go some way to alleviating these problems.[3] However, new device schemes operating on fundamentally different physical principles to the field effect transistor are needed to achieve higher processing speeds in combination with reduced levels of waste heat. A viable mechanism for this alternative technology to rival CMOS is spin current manipulation in hybrid metal/Ge semiconductor channels.[4,5] To utilize such spin currents in a voltage-controllable fashion, the spin-orbit coupling mechanism that leads to electric field tunable spin-splitting needs to be quantified in Ge quantum wells (QWs). This paper addresses this spin-splitting behaviour in applied magnetic fields and is set out in Secs. II–V. In Section II, device fabrication is discussed. Combinations of wet and dry etching were used to produce wide and narrow gated channels. In Section III, transport measurements are discussed on two wafer designs at 1.6 K and at 350 mK. In Section IV, a more detailed discussion and analysis of the spin-splitting in the resistivity is presented with a summary of the important points in Section V.

The spin-orbit coupling in bulk Ge valence band states, characterized by energy (Δ_o), does not directly translate into spin-orbit coupling of the free holes in a Ge quantum well system. In bulk Ge, $\Delta_o = 0.29\,eV$ and the spin-orbit split band with total angular momentum $\mathbf{J} = 1/2$ (with z-components $m_j = \pm 1/2$) is unoccupied by mobile holes. However, in the case of Ge quantum well channels ($\sim 10\,nm$ thickness) where the heavy hole (HH) band ($\mathbf{J} = 3/2$ with z-components $m_j = \pm 3/2$) forms the ground conducting state, there is no crystalline spin-orbit coupling (the Dresselhaus effect) as the diamond lattice of Ge does not have bulk inversion asymmetry (BIA). Recent measurements on Ge quantum wells have however indicated either a weak structural inversion asymmetry (SIA)-induced, cubic Rashba spin-orbit coupling effect due to electric fields in the growth direction[6–9] or a Zeeman effect.[10] These measurements were carried out at a higher carrier density than reported in this work. There is a fundamental difference between zero magnetic field spin-splitting with no overall spin-polarization and spin-splitting in a finite magnetic field. In an applied magnetic field, the spin-splitting caused by the Zeeman effect leads to a finite spin-polarization. The transport measurements in this paper were performed in a hole density regime where the strain-induced splitting (Δ) of the light ($m_j = \pm 1/2$) and heavy ($m_j = \pm 3/2$) hole valence band states is greater than the Fermi energy (E_f). The present measurements confirm that exchange enhanced Zeeman splitting is the main mechanism for spin-splitting in the compressively strained Ge quantum well. The spin-splitting in the heavy hole band should be qualitatively different to that from the light hole (LH) band where a spin-splitting, linear in momentum vector ($\mathbf{k}_{||}$) should be dominant.[11] As appealing as strained p-Ge appears to be for spintronic applications, the route to ambient temperature p-Ge quantum well nano-devices is still a hard challenge in terms of the choice for gate dielectrics and integration with silicon fabrication.[12]

II. DEVICE PREPARATION

A. Growth and processing

Ultra high hole mobilities have been achieved recently in the case of modulation doped, p-type Ge quantum wells.[13]

a)Author to whom correspondence should be addressed. Electronic mail: s.holmes@crl.toshiba.co.uk. Present address: Toshiba Research Europe Limited, Cambridge Research Laboratory, 208 Cambridge Science Park, Milton Road, Cambridge CB4 0GZ, United Kingdom.

120, 085702-1

This has been accomplished by incorporating a thin compressively strained Ge quantum well with SiGe barriers and a reverse-graded SiGe buffer layer on a standard silicon (001) substrate. Defects that introduce disorder and scattering are pinned away from the quantum well region. This procedure produces high mobility p-Ge QWs with ambient temperature values $\sim$4500 cm^2/V s, an order of magnitude larger than p-type doped Si.[14,15] The mobility is determined by background acceptor impurity scattering although interfaces and point defects can also limit the mobility; this is discussed in Section III B. The high quality growth process has been outlined in a series of publications over the last few years.[14,16] Polyimide was used as a gate dielectric with a nominal thickness of 430 nm after annealing at 300 °C for 60 min. Typical channel depletion voltages were $\sim$+2 V. Hall bar mesas were prepared using optical lithography with S1813 resist and dry etched with a CF$_4$ plasma. The Hall bar width was 75 μm, considerably larger than the lateral depletion width, determined to be $\sim$0.5 $\pm$ 0.1 μm in narrow wire arrays.[10] Narrow mesas from 3 μm to 1 μm structural width were also fabricated in this undoped material and are discussed in Section III E. Thermally evaporated Al was used as an Ohmic contact and annealed at 250 °C for 8 min. The contacts were Ohmic at low temperatures with contact resistance <1.6 kΩ per contact. The two wafers measured in this paper are insulating at low temperature (typically below 50 K) although a stable hole population of $\sim$1–2 $\times$ 10^{11} cm^{-2} can be induced in the quantum well by brief *in-situ* illumination. Reproducible resistivity measurements could be made when the carrier density was between $\sim$4 $\times$ 10^{10} cm^{-2} and $\sim$2 $\times$ 10^{11} cm^{-2}, corresponding to channel depletion and saturation, respectively. Wafers A and B differ only structurally in the Ge quantum well width and the SiGe barrier composition. Table I summarizes the electrical properties of the wafers determined from the low field Hall effect.

B. The band structure

The band structure of the undoped Ge quantum wells was modeled using the 8 band **k.p.** self-consistent device simulator[17] *nextnano*^{3}. Figure 1 shows the *nextnano*^{3} solution of the valence band at -1 V forward bias with a thick gate dielectric on wafer A. The band off-set between the Ge quantum well and the Si$_{0.3}$Ge$_{0.7}$ barriers for the heavy hole ground state is $\sim$0.26 eV. The solid black line is the self-consistent charge distribution with confinement to the 11 nm thick Ge quantum well. The heavy hole (HH) state forms the ground state with the unoccupied light hole (LH) state 94 meV higher in energy than the HH state. The Ge quantum well is compressively strained with a theoretical strain of 1.2% for the Ge well, Si$_{0.3}$Ge$_{0.7}$ barrier combination. However, the measured strain in the case of the Ge well, Si$_{0.2}$Ge$_{0.8}$ higher Ge content barrier
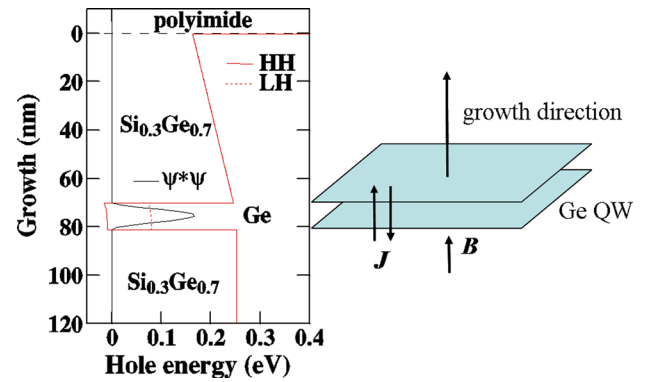

FIG. 1. The valence band structure of device A calculated using *nextnano*^{3} with a voltage of -1 V on the surface. The charge distribution $|\Psi * .\Psi|$ is plotted showing confinement to the Ge quantum well. The schematic shows the applied field and the quantization axis for **J** with respect to the growth direction and the applied magnetic field (**B**) direction.

structures is $\sim$0.65% due to a residual tensile strain in the barrier layer.[13] This effect will reduce Δ but not change the interpretation of the spin-splitting properties significantly.

III. MEASUREMENTS

A. Introduction to electrical measurements

The magnetotransport measurements were made between 1.6 K and 350 mK using either a standard ^{4}He variable temperature insert or a Heliox ^{3}He insert. The temperature was measured directly at the sample with a calibrated *Cernox* sensor in both cryostat systems. An AC excitation of between 10 and 100 nA was used for the source-drain current. Pre-amplifiers with $\times$100 gain and a 10 kHz bandwidth were used for ρ_{xx} and ρ_{xy} prior to lockin amplification at a frequency of 33 Hz. Gate voltages were applied with a Keithley 213 voltage source through a low pass filter.

B. The Hall effect

Figure 2(a) shows the Hall mobility (μ) as a function of hole density (p) at 1.6 K for wafer A. Three separate cool downs (labeled 1–3) are shown that demonstrate the reproducibility and stability of the persistent photoconductivity

TABLE I. The properties of the two wafers reported in this paper.

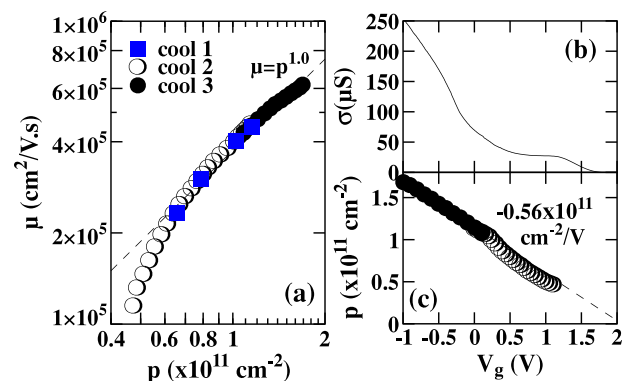| Wafer	Barrier material	QW width (nm)	p ($\times$10^{11} cm^{-2})	μ (cm^2/V s)
(A)	Si$_{0.3}$Ge$_{0.7}$	11	1.3	478 000
(B)	Si$_{0.2}$Ge$_{0.8}$	13	0.9	209 000

FIG. 2. (a) The Hall mobility as a function of hole density at 1.6 K *after* illumination in device A. Three separate cool downs are shown for comparison. (b) The two contact source-drain conductance and (c) hole density as a function of top gate voltage at 1.6 K in device A.

effect. The fact that $\mu \sim p^{1.0}$ prior to the on-set of insulating behaviour (for $p \sim 4 \times 10^{10}\,cm^{-2}$) indicates a dominant scattering mechanism due to residual background acceptor impurities in the quantum well and buffer layers.[18] The two contact source-drain conductance, including contact series resistance, is $\sim 70\,\mu S$ at V_g (top gate voltage) $= 0\,V$ although this can be increased to $250\,\mu S$ in enhancement without significant gate leakage current. Figure 2(b) shows the source-drain conductance after illumination showing a stable hole density. Full channel depletion is achieved at $\sim +2\,V$, with a capacitance of $-0.56 \times 10^{11}\,cm^{-2}/V$ from the Hall carrier density as a function of top gate voltage (see Figure 2(c)). This is close to the predicted capacitance value of $-0.42 \times 10^{11}\,cm^{-2}/V$, given the series capacitance contributions to the dielectric gate stack using the parameters in Table II and the following equation:

$$\left(\frac{dp}{dV_g}\right)^{-1} = e \cdot \left(\frac{d_{Ge}}{\varepsilon_{Ge}} + \frac{d_{SiGe}}{\varepsilon_{SiGe}} + \frac{d_{polyimide}}{\varepsilon_{polyimide}}\right), \quad (1)$$

where d is the layer thickness and ε is the dielectric constant. The variable subscripts refer to the different dielectric materials between the metal surface gate and the Ge quantum well. e is the unit of charge. This confirms the quantum well region is conducting rather than an interface or surface contribution. There is no screening of the gate field and no parallel conduction in the SiGe graded composition buffer layers or the Ge or Si cap at the surface. There is no drift of the pinch-off voltage or hysteresis in the conductivity versus gate voltage characteristic; i.e., there is no charge build-up at the surface of the polyimide dielectric.

C. The Shubnikov-deHaas effect

Magnetic fields (**B**) were applied in the growth direction, perpendicular to the conducting plane *and* parallel to the total angular momentum vector **J** (see Figure 1 for a schematic of the geometry). An ungated device from wafer A was measured at 350 mK (see Figure 3). This figure shows the Shubnikov-deHaas effect in ρ_{xx} and the quantum Hall effect in ρ_{xy} up to 1 T. The full data set was taken up to 12 T. A clear series of oscillations are observed down to filling factors υ (h·p/eB) ~ 15, where h is Planck's constant with a single fundamental field (B_f) of 2.65 T, corresponding to $p = 1.28 \times 10^{11}\,cm^{-2}$. The inset of Figure 3 is a plot of the filling factor against inverse minima field position ($1/B_\upsilon$), showing that a single harmonic series is present with no evidence of beating, multiple frequencies or a second subband. The gradient of the line corresponds to the measured B_f value. The grey area in Figure 3 inset shows the region where quantum Hall plateaus are observed (with $\rho_{xy} = h/\upsilon e^2$), confirming the unique filling factor assignment. A fast Fourier transform

TABLE II. Dielectric properties associated with wafer A.

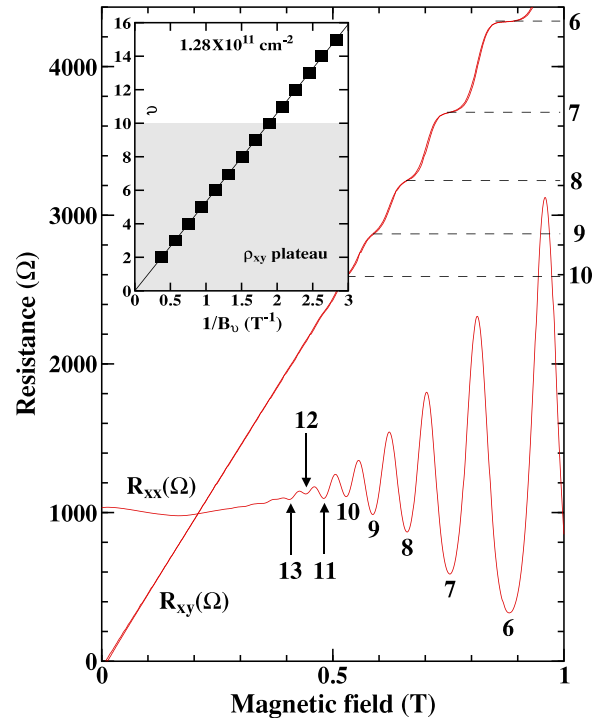| Material	d (nm)	ε_r
Ge	8.5	16.0
$Si_{0.3}Ge_{0.7}$	70	14.8
polyimide	430	3.4

FIG. 3. ρ_{xx} and ρ_{xy} at low field and 360 mK in (ungated) device A after illumination showing the prevalence of odd-minima in ρ_{xx} at the on set of the oscillations. The inset shows the filling factor as a function of the position of the Shubnikov-deHaas minima in 1/B. The shaded area corresponds to the observation of quantum Hall effect plateaux.

(FFT) of the oscillations in ρ_{xx} shows a single fundamental field at $B_f = h \cdot p/e$ due to the dominance of *odd* filling factors in the Shubnikov-deHaas effect in the low field region. The lowest visible minima are at odd filling factors 13, 15, 17; this point is further discussed in Section IV and is fundamental to understanding the spin-splitting behaviour in p-Ge. Any non-parabolicity in the Ge valence band could introduce harmonics of B_f in the FFT, but these are not seen at this hole density, where $E_f \sim 2.7\,meV$. Non-sinusoidal Shubnikov-deHaas oscillations included in the field domain of the FFT can also produce additional harmonic peaks as previously reported[7] in p-Ge.

A magnetic field modulation system was used to measure analogue dR_{xx}/dB and d^2R_{xx}/dB^2 signals directly. A solenoid co-linear with the DC magnetic field was used that provided an AC magnetic field of 5.7 mT at 33 Hz. A lock-in amplifier was used to measure dR_{xx}/dB at the fundamental 33 Hz. The second harmonic signal at 66 Hz corresponds to d^2R_{xx}/dB^2. The R_{xx} and $-d^2R_{xx}/dB^2$ signals can be compared on the same plot, for example, Figure 4. The sensitivity of the magnetic field modulation technique in measuring device B is demonstrated in Figure 4. The red curve is the DC ρ_{xx} at 0.4 K and the green curve is the DC ρ_{xx} at 1.6 K. At 1.6 K, even filling factor Shubnikov-deHaas minima > 4 and odd minima > 7 have disappeared in ρ_{xx}. In the analogue second derivative signal at 1.6 K (the dotted green curve), odd minima can still be observed for $\upsilon > 7$ showing the increased sensitivity to oscillatory ρ_{xx} structure. The random noise level in Figure 4 is less than the width of the red and green lines. There are *no* multiple frequencies (i.e., peak splitting) in the FFT of dR_{xx}/dB or d^2R_{xx}/dB^2 from device A or B that would be characteristic of a Rashba spin-splitting.
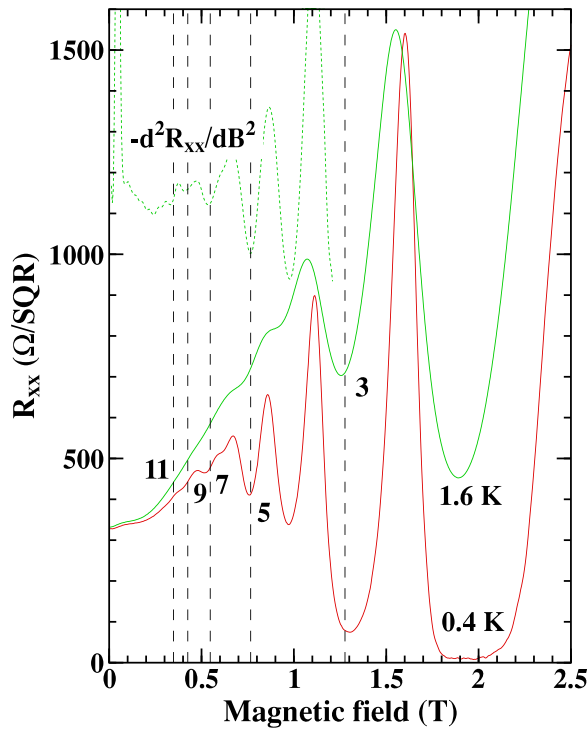
FIG. 4. Magnetoresistance in device B with carrier density $9 \times 10^{10}\,\mathrm{cm}^{-2}$. The odd filling factors (from 3 to 11) are indicated by the vertical dotted lines. The y-axis scale in the case of $-d^2R_{xx}/dB^2$ is in arbitrary units not the Ω/SQR units of the labeled y-axis. SQR is the length to width ratio of the Hall bar.
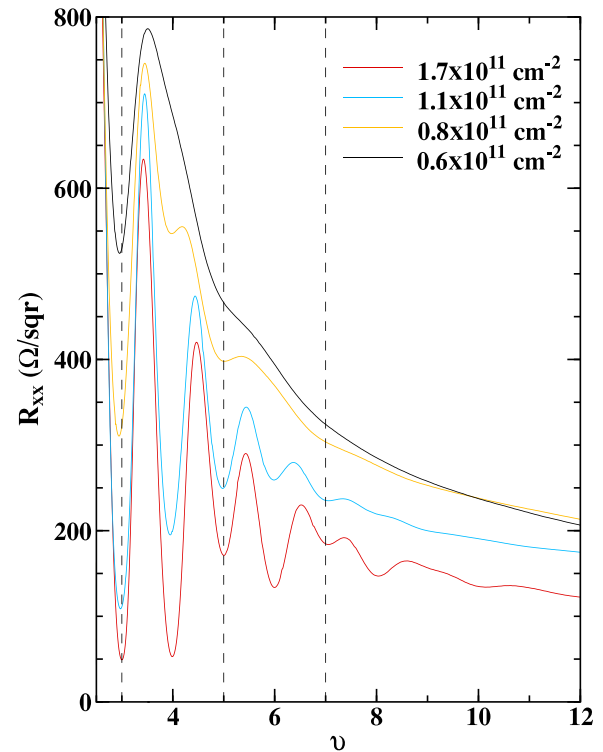

FIG. 5. ρ_{xx} measurements at 1.6 K as a function of filling factor in device A showing the development of the *even* filling factors with increasing hole density. At $6 \times 10^{10}\,\mathrm{cm}^{-2}$, only odd minima are observed at $\upsilon = 3, 5,$ and 7 (the vertical dashed lines).

D. Gated transport measurements

In Figure 5, ρ_{xx} is plotted as a function of filling factor in a series of gated measurements at 1.6 K in device A. At $0.6 \times 10^{11}\,\mathrm{cm}^{-2}$ Shubnikov-deHaas minima are observed at $\upsilon = 3, 5,$ and 7 (the vertical dotted lines) with an even minimum only at the Shubnikov-deHaas fundamental $\upsilon = 2$ position, not shown in the figure. Even minima (>2) start to develop as the carrier density is increased with the surface gate, for example, the $\upsilon = 6$ minimum starts to appear at $1.1 \times 10^{11}\,\mathrm{cm}^{-2}$. The dominance of odd minima is due to the large g-factor (g) in the HH states of the Ge valence band with the Zeeman splitting $(\Delta E_{ss}) = 3\,g\mu_B B$, comparable to the cyclotron energy ($\hbar eB/m^*$) in this material where m^* is the effective hole mass and μ_B is the Bohr magneton. This is discussed further in Section IV. The reduction of the energy gap at even filling factors in the Shubnikov-deHaas effect has been previously observed in lower mobility p-Ge super-lattices[19] and p-SiGe quantum wells.[20] The effect is clearer in lower mobility material with larger Landau level broadening and is relatively unnoticed when p is $>1.7 \times 10^{11}\,\mathrm{cm}^{-2}$. At $\sim 2 \times 10^{11}\,\mathrm{cm}^{-2}$ in the modulation doped Ge quantum well system,[10] the prevalence of odd minima has gone although the spin-splitting is still the dominant exchange enhanced Zeeman effect.

Low filling factors were investigated in these wafers in magnetic fields up to 12 T. A fractional quantum Hall effect (fqhe) is observed at 350 mK corresponding to $\upsilon = 2/3$ (at higher carrier density) and 1/3 (at lower carrier density) in device A. The momentum scattering rate $1/\tau_p$

(where τ_p is the momentum lifetime calculated from the transport mobility) is in the region of $\sim 70\,\mathrm{GHz}$ or less to observe the fqhe as a general rule from the literature over a range of semiconducting materials.[21] This corresponds to a $\mu > 300\,000\,\mathrm{cm}^2/\mathrm{V\,s}$ for the case of heavy holes in Ge, easily achieved with p as low as $\sim 0.8 \times 10^{11}\,\mathrm{cm}^{-2}$ in device A.

In wafer A at high magnetic field (and 350 mK), a magnetoresistance characteristic of the fqhe can be seen developing in the lowest Landau level (see Figure 6). This figure shows σ_{xx} and σ_{xy} as a function of the filling factor at 350 mK from $p = 0.78$ to $1.6 \times 10^{11}\,\mathrm{cm}^{-2}$. Minima can be seen developing at 2/3 and 1/3 in σ_{xx}. These minima correspond to the formation of fractional plateau in σ_{xy} at $2/3(e^2/h)$ and $1/3(e^2/h)$. Higher mobility p-Ge material from the same growth system has shown a richer fqhe structure in the second Landau level[22] at lower temperatures and the low filling factor regime is not discussed further here.

E. Narrow channel arrays

In a narrow channel, the loss of even filling factors in the Shubnikov-deHaas effect is even more pronounced. Figure 7 shows the magnetoresistance in an array of narrow channels with nominal physical widths of 3, 2, and 1 μm from wafer A. The inset shows a low field FFT of the Shubnikov-deHaas oscillation in this device with the fundamental field at $h \cdot p/e$ due to the dominant Zeeman splitting enhancing the odd filling factor minima in comparison to the even minima. The influence of the increased scattering rate in the 2 and 1 μm device channels can be seen as a clear loss of the minima at $\upsilon = 4$, leaving only a strong 3
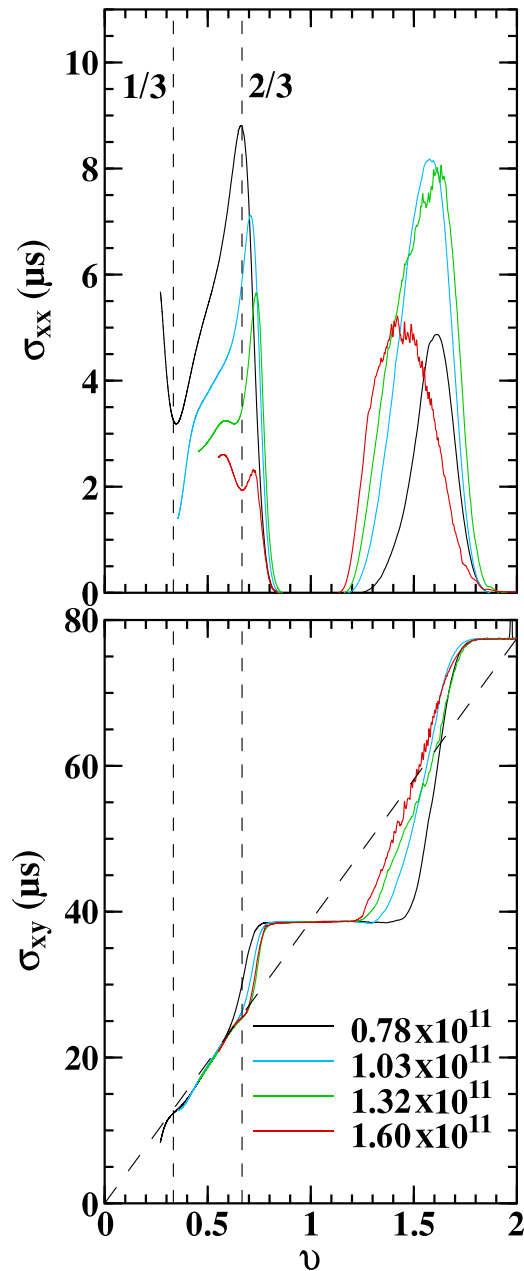
FIG. 6. σ_{xx} and σ_{xy} as a function of the filling factor at 350 mK for hole densities from 8×10^{10} cm^{-2} to 1.6×10^{11} cm^{-2} in device A. The maximum applied magnetic field is 12 T. The dashed diagonal line in σ_{xy} corresponds to $\upsilon e^2/h$.

and 5 (and 7) minima. This behavior is also confirmed when analogue $d\rho_{xx}/dB$ signals are directly measured by magnetic field modulation or by increasing the measurement temperature. The saturation carrier density does not change with wire width due to the low density of surface states at the etched Ge sidewall.[10] The conducting wire width as opposed to the lithographic wire width could not be determined as the low field boundary scattering peak (see Ref. 10) was not well defined. However, the field extent over which a negative magnetoresistance dominates does increase from 0.2 to 0.4 T (in Fig. 7) with decreasing mesa width but without quantitative numbers available for the conducting thickness and the depletion width.
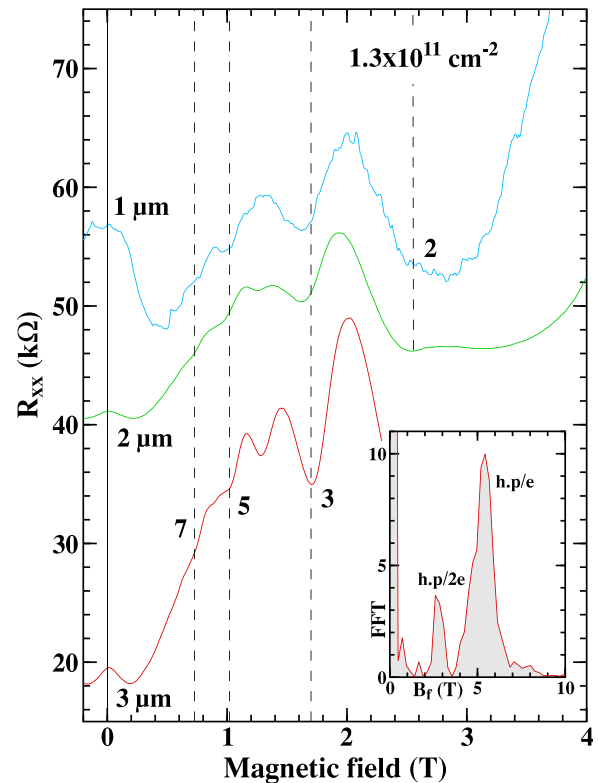

FIG. 7. ρ_{xx} up to 4 T in a series of narrow channels (width 1 to 3 μm as indicated) at 1.6 K from wafer A showing the suppression of the $\upsilon = 4$ minima with increasing disorder. The filling factors are labeled as dashed lines. The inset shows the FFT of ρ_{xx} from the 3 μm wide channel.

IV. DISCUSSION

A. Zero magnetic field spin-splitting

The Ge quantum well is compressively strained and has HH ($J = 3/2$, $m_j = \pm 3/2$) character at the top of the valence band with the LH states ($J = 3/2$, $m_j = \pm 1/2$) higher in energy. In Section II, this HH-LH energy splitting was calculated as 94 meV; hence, there is a negligible LH contribution to the charge transport. The Rashba term in the Hamiltonian[23,24] for the Γ_{8v} states is given by

$$\hat{H}_{\Gamma 8v}^{Rashba} = \beta_1 (\boldsymbol{k}_{||} \times \boldsymbol{E}) \cdot \boldsymbol{J} + \beta_2 (\boldsymbol{k}_{||} \times \boldsymbol{E}) \cdot \boldsymbol{J}^3, \qquad (2)$$

where the total angular momentum $\boldsymbol{J}$ has components (J_x, J_y, J_z), $\boldsymbol{J}^3$ has components, (J_x^3, J_y^3, J_z^3), and $\boldsymbol{k}_{||}$ has components $(k_x, k_y, 0)$. The electric field $\boldsymbol{E}$ is in the growth direction with components $(0, 0, E_z)$. In Eq. (2), $\beta_1 \gg \beta_2$ with no linear k, spin-splitting for the HH band.[23] The HH spin-splitting is then given by: $\Delta E_{ss} = 2\beta_1 k_{||}^3$. However, the fundamental quantization axis for the angular momentum $\boldsymbol{J}$ is along the strain vector, perpendicular to the plane of the Ge quantum well. This means that the ground state HH spin orientation is out of plane with the higher energy LH spin states projected in-plane. If the in-plane momentum is $\boldsymbol{k}_{||}$, then for a perpendicular electric field $\boldsymbol{E}$

$$(\boldsymbol{k}_{||} \times \boldsymbol{J}) \cdot \boldsymbol{E} \approx 0; \ \boldsymbol{k}_{||} \cdot \boldsymbol{J} \approx 0, \qquad (3)$$

and a Rashba spin-splitting cannot exist in the strained QW for the out-of-plane HH angular momentum orientation. This

partly explains the lack of Rashba spin-splitting in devices where there is negligible coupling to the LH states. In Figure 8(a), the calculated band structure for the HH state is plotted as a function of in-plane momentum (k_x or k_y) assuming m* = 0.09·m_e from Ref. 25 and a β_1 value of 100 eV Å^3 from Ref. 7. The spin projection conserves time reversal symmetry with the state at energy E(+k, ↑) = E(−k, ↓). In Figure 8(b), the energy splitting ΔE_{ss} = E(k, ↑) − E(k, ↓) is plotted as a function of k. The vertical dotted lines correspond to the Fermi wave vector for p = 1 × 10^{11} cm^{-2}. Two values of β_1 are used from the literature, 20 eV Å^3 (the highest value measured in Ref. 6) and 100 eV Å^3 (Ref. 7) as a comparison. The predicted spin-splitting at 1 × 10^{11}cm^{-2} is in the range 0.02 meV–0.1 meV. The ΔE_{ss} value corresponds to a thermal energy k_B·T (where k_B is Boltzmann's constant and T is the temperature) of 0.23 K (with β_1 from Ref. 6) with the actual measurement temperature of ∼7 × ΔE_{ss} and hence a thermal broadening of any potential Rashba effect.

The previous theoretical work on the Rashba effect[23,24] in the valence band predicts a cubic Rashba effect for the HH state but ignores the fact that strain provides the main quantization axis for the angular momentum states. In the Ge quantum well, the SIA contribution to the spin-splitting is controlled by the effective potential steps at the Ge-Si$_{1−x}$Ge$_x$ interfaces and there is very little contribution from the applied gate voltage or the built-in electric field in
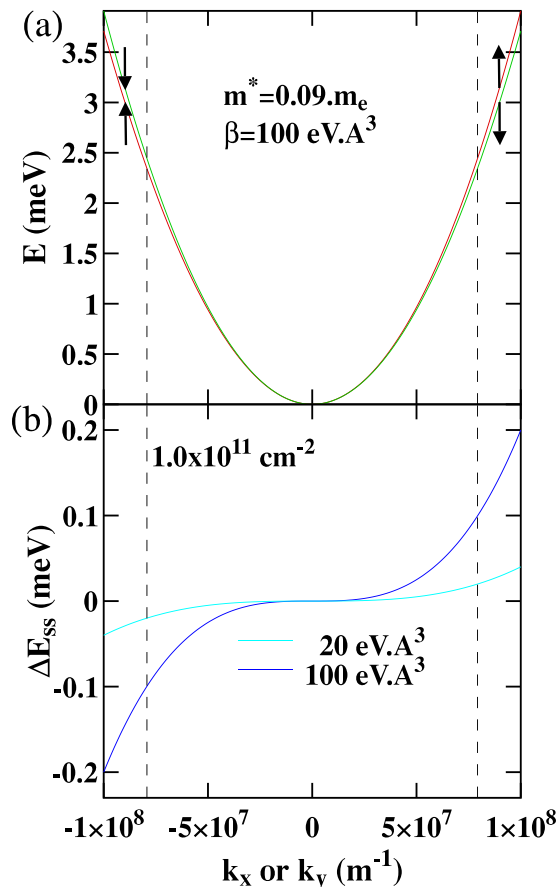

FIG. 8. (a) The band structure in the heavy hole band in Ge for β_1 = 100 eV Å^3, showing the ±3/2 angular momentum states. (b) The spin-splitting energy as a function of in-plane wave vector with the predicted β_1 parameter from Refs. 6 and 7 for comparison.

determining the spin-splitting, i.e., ΔE_{ss} should be insensitive to the applied gate voltage. Previous experimental measurements[6–9] have demonstrated a small to moderate Rashba effect with only a weak dependence on applied electric field, in disagreement to what is measured here.

B. Spin-splitting in finite magnetic field

The Zeeman energy term for the overall Luttinger Hamiltonian[26] in the valence band with J = 3/2 in an applied perpendicular magnetic field B is given by the following equation:

$$\hat{H}_{\Gamma 8v}^{Zeeman} = 2\kappa\mu_B B \cdot J + 2q\mu_B B \cdot J^3. \quad (4)$$

The first term in Eq. (4) is an isotropic term (with axial symmetry defined by **J**) and this dominates over the second anisotropic term. 2κ is the g-factor, determined from the Luttinger formulation,[24,26] and the band parameter q is calculated from **k·p** theory. This is an energy correction due to coupling to remote (conduction) bands. In the Ge HH valence band, q ≪ κ and Eq. (4) reduces to $\hat{H}_{\Gamma 8v} = g\mu_B B \cdot J$ with $\Delta E_{ss} = 3g\mu_B B$ the dominant spin-splitting term in an applied magnetic field. In the Luttinger model,[24,26] the mixing of HH-LH states in applied magnetic field is negligible unless there is a magnetic field component in-plane. Previous measurements[27] on acceptor states in narrow Ge quantum wells have made use of the fact that an in-plane magnetic field can split the LH states while preserving the HH (m_j = ±3/2) degeneracy.

The effective mass[7,25] and the g-factor[25,28] have been determined in p-Ge as 0.09 ± 0.02 m_e with g in the range from 4 to 7. With these parameter values from the literature, the Zeeman splitting is comparable to the cyclotron energy splitting, with $\frac{\Delta E_{ss}}{\hbar\omega_c} = \frac{3}{2}g\frac{m^*}{m_e} \approx 0.8\pm0.4$, where the cyclotron frequency ω_c = eB/m*. This leads to the dominant anomalous Zeeman splitting effect particularly at odd filling factors that are observed in Figure 5. The Zeeman spin-split peak of the Shubnikov-deHaas oscillation FFT is then at h·p/e. This frequency identification in the Shubnikov-deHaas effect can be seen in the inset of Figure 7. The dominance of odd minima in the Shubnikov-deHaas effect disappears for p ∼ 2 × 10^{11} cm^{-2}. This is for two reasons. First, the "disordered" Landau level width is proportional to B$^{-1/2}$, so at higher hole density the Shubnikov-deHaas minima occur at higher real B and the Landau levels have a reduced width. This would tend to reverse the effects of losing the even filling factor gaps in the density of states at low carrier density. The second effect is that influenced by the exchange interaction. The Landé g-factor that determines the Zeeman energy gap is exchange energy enhanced, and at higher B, the exchange energy reduces (there is less spatial wavefunction overlap) decreasing the Zeeman energy gap. This would have the effect of increasing the dominance of even minima gaps that can be seen developing at p ≈ 1.7 × 10^{11} cm^{-2} in Figure 5.

V. SUMMARY

The compressively strained Ge quantum well guarantees that the out-of-plane heavy hole angular moment component

$m_j = \pm 3/2$ does not couple to the linear in-plane momentum via a linear (or cubic) Rashba spin-orbit effect with $p \sim 10^{11} \, \text{cm}^{-2}$. There is no measurable Rashba spin-orbit coupling unless there is HH-LH mixing of the wavefunction caused by compressive strain, high p-type doping, or applied in-plane magnetic field. In the compressively strained Ge quantum well-SiGe barrier combination, this mixing effect is ruled out by the large energy splitting between the $m_j \pm 3/2$ and $\pm 1/2$ states. The dominance of odd minima ρ_{xx} in the Shubnikov-deHaas effect is due to the anomalous Zeeman splitting of the heavy hole state compared to the cyclotron energy. The effects reported in this work are also applicable in the $In_xGa_{1-x}Sb$-GaSb strained p-type quantum well system, where the heavy hole spin state is projected in the growth direction, leading to spin confinement.[29] Undoped p-Ge strained quantum wells behave as a spin $\pm 3/2$ system with the spins oriented in the strain (growth) direction. Any Rashba spin-orbit coupling effect is likely to be due to LH states that can be occupied depending on the details of the strain in the device, the confining potential, and the p-type doping level.

ACKNOWLEDGMENTS

[1]See http://www.itrs2.net/2013-itrs.html for International Technology Roadmap for Semiconductors (ITRS2).

[2]I. L. Markov, Nature **512**, 147 (2014).

[3]P. S. Goley and M. K. Hudait, Materials **7**, 2301 (2014).

[4]C. Shen, T. Trypiniotis, K. Y. Lee, S. N. Holmes, R. Mansell, M. Husain, V. Shah, H. Kurebayashi, I. Farrer, C. H. de Groot, D. R. Leadley, G. Bell, E. H. C. Parker, T. Whall, D. A. Ritchie, and C. H. W. Barnes, Appl. Phys. Lett. **97**, 162104 (2010).

[5]S. Dushenko, M. Koike, Y. Ando, T. Shinjo, M. Myronov, and M. Shiraishi, Phys. Rev. Lett. **114**, 196602 (2015).

[6]R. Moriya, K. Sawano, Y. Hoshi, S. Masubuchi, Y. Shiraki, A. Wild, C. Neumann, G. Abstreiter, D. Bougeard, T. Koga, and T. Machida, Phys. Rev. Lett. **113**, 086601 (2014).

[7]C. Morrison, P. Wisniewski, S. D. Rhead, J. Foronda, D. R. Leadley, and M. Myronov, Appl. Phys. Lett. **105**, 182401 (2014).

[8]J. Foronda, C. Morrison, J. E. Halpin, S. D. Rhead, and M. Myronov, J. Phys.: Condens. Matter **27**, 022201 (2015).

[9]M. Failla, M. Myronov, C. Morrison, D. R. Leadley, and J. Lloyd-Hughes, Phys. Rev. B **92**, 045303 (2015).

[10]P. J. Newton, J. Llandro, R. Mansell, S. N. Holmes, C. Morrison, J. Foronda, M. Myronov, D. R. Leadley, and C. H. W. Barnes, Appl. Phys. Lett. **106**, 172102 (2015).

[11]R. Winkler, D. Culcer, S. J. Papadakis, B. Habib, and M. Shayegan, Semicond. Sci. Technol. **23**, 114017 (2008).

[12]R. Pillarisetty, Nature **479**, 324 (2011).

[13]A. Dobbie, M. Myronov, R. J. H. Morris, A. H. A. Hassan, M. J. Prest, V. A. Shah, E. H. C. Parker, T. E. Whall, and D. R. Leadley, Appl. Phys. Lett. **101**, 172108 (2012).

[14]M. Myronov, C. Morrison, J. Halpin, S. Rhead, C. Casteleiro, J. Foronda, V. A. Shah, and D. Leadley, Jpn. J. Appl. Phys., Part 1 **53**, 04EH02 (2014).

[15]M. Myronov, C. Morrison, J. Halpin, S. Rhead, J. Foronda, and D. R. Leadley, Solid-State Electron. **110**, 35 (2015).

[16]O. A. Mironov, A. H. A. Hassan, R. J. H. Morris, A. Dobbie, M. Uhlarz, D. Chrastina, J. P. Hague, S. Kiatgamolchai, R. Beanland, S. Gabani, I. B. Berkov, M. Helm, O. Drachenko, M. Myronov, and D. R. Leadley, Thin Solid Films **557**, 329 (2014).

[17]See http://www.nextnano.de/nextnano3/ for nanodevice simulator software, *nextnano³*.

[18]A. Gold, Phys. Rev. B **35**, 723 (1987).

[19]Yu. G. Arapov, N. A. Gorodilov, V. N. Neverov, G. I. Kharus, N. G. Shelushinina, O. A. Kuznetsov, L. K. Orlov, R. A. Rubtsova, and A. L. Chernov, JEPT Lett. **59**, 245 (1994).

[20]P. T. Coleridge, A. S. Sachrajda, H. Lafontaine, and Y. Feng, Phys. Rev. B **54**, 14518 (1996).

[21]B. A. Piot, J. Kunc, M. Potemski, D. K. Maude, C. Bethausen, A. Vogl, D. Weiss, G. Karczewski, and T. Wojtowicz, Phys. Rev. B **82**, 081307(R) (2010).

[22]Q. Shi, M. A. Zudov, C. Morrison, and M. Myronov, Phys. Rev. B **91**, 241303(R) (2015).

[23]R. Winkler, H. Noh, E. Tutuc, and M. Shayegan, Phys. Rev. B **65**, 155303 (2002).

[24]R. Winkler, Phys. Rev. B **62**, 4245 (2000).

[25]I. B. Berkutov, V. V. Andrievskii, Yu. F. Komnik, O. A. Mironov, M. Myronov, and D. R. Leadley, Low Temp. Phys. **35**, 141 (2009).

[26]J. M. Luttinger, Phys. Rev. **102**, 1030 (1956).

[27]K.-M. Haendel, R. Winkler, U. Denker, O. G. Schmidt, and R. J. Haug, Phys. Rev. Lett. **96**, 086403 (2006).

[28]J. C. Hensel, Phys. Rev. Lett. **21**, 983 (1968).

[29]R. W. Martin, R. J. Nicholas, G. J. Rees, S. K. Haywood, N. J. Mason, and P. Walker, Phys. Rev. B **42**, 9237 (1990).